Efficient Randomly Encoded Data Acquisition for Compressed Sensing

E. C. Wong[1]
[1]Radiology and Psychiatry, UC San Diego, La Jolla, CA, United States

Introduction

Compressed sensing (CS) technology (1) has demonstrated that it is useful to focus on the information content in MR imaging data, rather than specifically fulfilling the Nyquist sampling criterion. We revisit here the desired properties of efficient MR data acquisition, beginning with the following observations: 1) CS reconstruction calls for sampling functions that are incoherent (dense) in the sparse domain; 2) SNR efficiency is maximized with high steady state transverse magnetization and high A/D duty cycle, as exemplified by balanced SSFP; 3) In clinical MRI, images of the same anatomy with different image contrast are often acquired, and the mutual information between these images is high. In response to these criteria, we propose the following imaging strategy.

Methods

1) Short TR imaging with random phase RF. Random phase RF pulses can produce similar steady state transverse magnetization to balanced SSFP, but the magnitude of the response is independent of resonance offset, and the peak response for physiological T_1 and T_2 values occurs at much lower flip angle. At T_1=1000ms, T_2=50ms, and TR=1ms, 2° random phase or 40° phase alternating pulses both produce a steady state RMS M_{xy} of approximately $0.1M_0$.

2) A low peak curvature gradient trajectory for rapid sampling of spatial information that re-circulates in a conventional sized patch of k-space with RF pulses applied at random locations near the center of the trajectory. After many pulses this generates a distribution of coherences, which produces spatially random excitation with feature sizes that are controllable by the distribution of pulses, and has dense representations in most transform domains. Excitation in any particular voxel is modulated randomly in time, which encodes T_1 and T_2 data into the signal. The rosette trajectory (2) with nearly circular petals is an example of a trajectory with low curvature and allows for rapid continuous k-space traversal.

3) Simultaneous estimation of proton density, relaxation times, and resonance offset using CS methods. Data was simulated using direct integration of the Bloch equations and the following parameters: real human source images of proton density T_1, and T_2 at 64x64 resolution; synthesized quadratic field map with peak offset of 3Hz; 64 petals with 64 points collected on each petal; 10μs per data point for a total scan time of 41ms; one 4° rf pulse per petal, with a Gaussian distribution with σ=0.25*kmax.

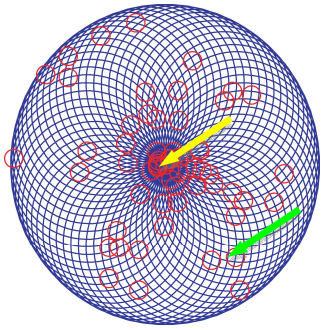

Figure 1: Gradient trajectory (blue) and RF pulses (red). Arrows discussed below.

Reconstruction was by iterative minimization using conjugate gradient descent and numerical calculation of gradients. The cost function was:

$$C(pd,T_2,f)=\left\|F(pd,T_2,f)-y\right\|_{l_2}^2+\lambda_1\left\|W(pd)\right\|_{l_1}+\lambda_2 TV(pd)$$

where pd is the proton density, f is the field map, y is the simulated data, F() generates simulated data, W() is a wavelet transform, and λ_n are adjusted so that the contributions to C are on the same order. In addition, the gradient of the field map was smoothed with a Gaussian kernel with σ=9 pixels at each iteration, and 200 iterations were used.

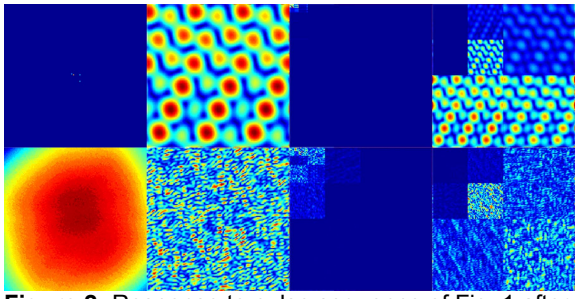

Figure 2: Response to pulse sequence of Fig. 1 after 4 (top) and 64 (bottom) RF pulses. From left: Relative density of transverse coherences in k-space; M_{xy} in image space; Wavelet transform of M_{xy} at points indicated by yellow and green arrows in Fig. 1.

Results

An example rosette trajectory is shown in **Figure 1** with random phase 2° RF pulses applied at the red circles. For this pulse sequence, the state of the spin system after the 4th and 64th RF pulses is shown in **Figure 2**. After 4 pulses the FIDs of the pulses dominate the coherences, as echo pathways are slow to build up when the flip angles are small. After 64 pulses a nearly continuous distribution of coherences exists, but with random phases. The magnetization is noise like in image space, and the wavelet representation of the sampling function is relatively dense compared to that of Fourier basis functions. **Figure 3** shows the original and reconstructed proton density, T_2, and field maps. These 3 maps are estimated using 64^2 data points, equal to the number of pixels in one map.

Discussion

The approach proposed here simultaneously produces high steady state signal, high A/D duty cycle, and pseudo-random sampling functions, and is therefore both SNR efficient and amenable to CS reconstruction. Because the mutual information between pd, T_1, and T_2 is high, simultaneous estimation of pd, T_1, and T_2 should be more efficient than separate acquisition of the same anatomy with different contrasts, and it is natural to add mutual information to the cost function. The distribution of coherences is controlled by the distribution of RF pulses and by the flip angle, which determines the weighting of echo pathways, and there is a tradeoff in which the randomness of the sampling function improves with a broader coherence distribution, but eventually leads to signal loss due to intravoxel dephasing. Extension to 3D is straightforward, and it is expected that sparsity in the wavelet domain will increase with dimension and resolution. Using this approach, 256^3 data points can be collected in approximately 1min with current gradient hardware, and the rapid acquisition of high resolution volumetric anatomical and parameter maps is an ultimate goal of this work.

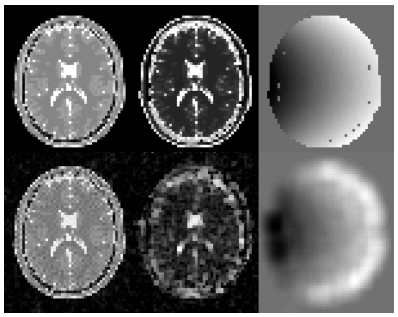

Figure 3: Top: Source images; Bottom: Images reconstructed from simulated data. From left: proton density, T_2, field map

References

1. Lustig et al MRM 58:1182 2007.
2. Noll, *IEEE TMI* **16:**372 1997.